Journal of Advances in Mathematics and Computer Science

xx(x): ....., 20yy; Article no.JAMCS.xxxxx

ISSN: 2456-9968

(Past name: British Journal of Mathematics & Computer Science, Past ISSN: 2231-0851)

Exact Solution of MHD Pulsatile Flow of Couple-Stress fluid through Porous Medium

Original Research Article

Abstract

The present paper examines the MHD pulsating flow of a couple-stress fluid in a high-permeability porous medium sandwiched between two permeable beds. The Brinkmann equation models flow in the porous channel, while Darcy's law describes flow in permeable beds. The porous medium has high permeability, so the Beaver-Joseph boundary condition is used at the permeable beds. The governing partial differential equation of flow, along with boundary conditions, is separated into steady and oscillatory parts. The analytical solutions have been derived for fluid velocity, shear stress at permeable beds, and mass flux. The impact of governing flow parameters on the fluid velocity and shear stress is illustrated through graphs and tables.

Keywords: Non-Newtonian Fluids; Pulsatile flow; Permeable beds; Porous medium; Magneto-hydrodynamic Flow

2010 Mathematics Subject Classification: 76S05.

1 Introduction

Flow through porous media remains a topic of interest among researchers due to its numerous applications in natural and artificial processes. The natural processes include groundwater flow, flow of hydrocarbons in petroleum wells, blood flow in biological tissues, etc. Medical engineering, Mechanical engineering, Chemical engineering, and other branches of engineering are areas where flow through porous media plays a vital role. The study of flow through porous media also plays a major role in industries like the paper and wood industry, the food processing industry, the petroleum, oil and gas industry, etc.

In 1967, Beaver and Joseph [1] presented boundary conditions for naturally permeable porous media, known as the Beaver-Joseph boundary condition. The boundary condition is very useful in

modelling the clear fluid flow over a porous region. Chang Yi Wang [2] has done a detailed study on pulsatile flow in porous media. Rudraiah et.al. [3] discussed Hartmann flow over a permeable bed in the presence of a transverse magnetic field. They considered an interface at the surface of the permeable bed. G. Radhakrishnamacharya and M. K. Maithi [4] studied heat transfer in a pulsatile flow between two infinitely long parallel porous plates. Pulsatile flow in circular tubes of varying cross sections has been investigated by Piyush Chandra and J.S.V.R.K. Prasad [5]. They used perturbation techniques to find the solution. S.A.N. Elsoud [6] studied the interaction between a couple stress fluid and a peristaltic flow. K. Vajravelu et.al. [7] discussed pulsatile flow of a viscous Newtonian fluid between two permeable beds with constant injection from the lower permeable bed and constant suction from the upper permeable bed. N.A.S. Affifi and N.S. [8] Gad studied peristaltic fluid with a pulsatile Newtonian fluid through a porous medium. T. Malathy and S. Srinivas [9] did a thorough investigation of a hydro-magnetic fluid between two permeable beds with uniform injection and suction. They found that for a specific choice of parameters, the velocity can attain its maximum at the lower permeable bed. A. Pantokratoras and T. Fang [10] investigated fully developed flow of an electrically conducting fluid in a saturated porous medium channel and derived exact analytical solutions. Flow through a porous medium between permeable beds under an exponentially decaying pressure gradient was discussed in detail by B.G. Prasad and A. Kumar [11]. The pulsatile flow of a viscous stratified fluid with variable viscosity between two permeable beds was investigated by K. Avinash et al. [12]. Srinivasacharya and Rao [13] discussed the influence of magnetohydrodynamics on the flow of a couple-stress fluid through a bifurcated artery. The flow of a couple-stress fluid due to slow steady oscillations of a permeable sphere is investigated by Aparna et al. [14]. Exact analytical solutions for the Navier–Stokes equations with couple stresses were examined by E.S. Baranovskii et al. [15]. Deepak Kumar and Manju Agarwal [16] discussed the flow of two immiscible couple-stress fluids in a channel between two permeable beds. The rheology of peristaltic flow of a couple stress fluid in an inclined tube with heat and mass transfer effects has been investigated by Abbas et al. [17]. Tarakaramu et al. [18] studied three-dimensional couple-stress fluid flow over a permeable stretching sheet with non-linear thermal radiation and heat source effects. Alsudais et al. [19] examined the Stokes flow of an incompressible couple-stress fluid confined between two eccentric spheres. Recently, an unsteady 2-D laminar flow of magnetohydrodynamic fluid generated by an elastic surface immersed in a permeable medium under the influence of thermal radiation with temperature dependent thermal conductivity and viscosity was studied by S Bansal, RS Yadav [20]. S.R. Dhwal [21] investigated a non-Newtonian radiating Casson fluid in a Darcy-Forchheimer porous medium over a slippery, permeable surface.

Couple-stress fluids are a type of non-Newtonian fluids that consider the effect of microscopic particle rotations and internal couple stresses. These factors are crucial in fluids with micro-structure. The flow of couple stress fluids in a porous medium has wide applications in bio-mechanics, lubrication theory, and enhanced oil recovery, where internal couple stresses have a significant impact on flow resistance and transport behaviour. A magnetohydrodynamic pulsating flow of a couple-stress through a high-permeability porous medium sandwiched between two permeable beds is investigated in the present paper.

2 Mathematical Formulation

The geometry under consideration, given in Figure 1, consists of a flow of couple stress fluid inside a rectangular porous channel of high permeability between two permeable beds with uniform injection and suction. The couple stress fluid, flowing in the region $0 \leq y \leq h$, has density ρ, viscosity μ, couple stress viscosity η, and electrical conductivity σ. The permeability of the porous region is K, while K_1 and K_2 are the permeabilities of the lower and upper permeable beds, respectively. The flow is governed by a pulsating pressure gradient under the influence of a transverse magnetic field

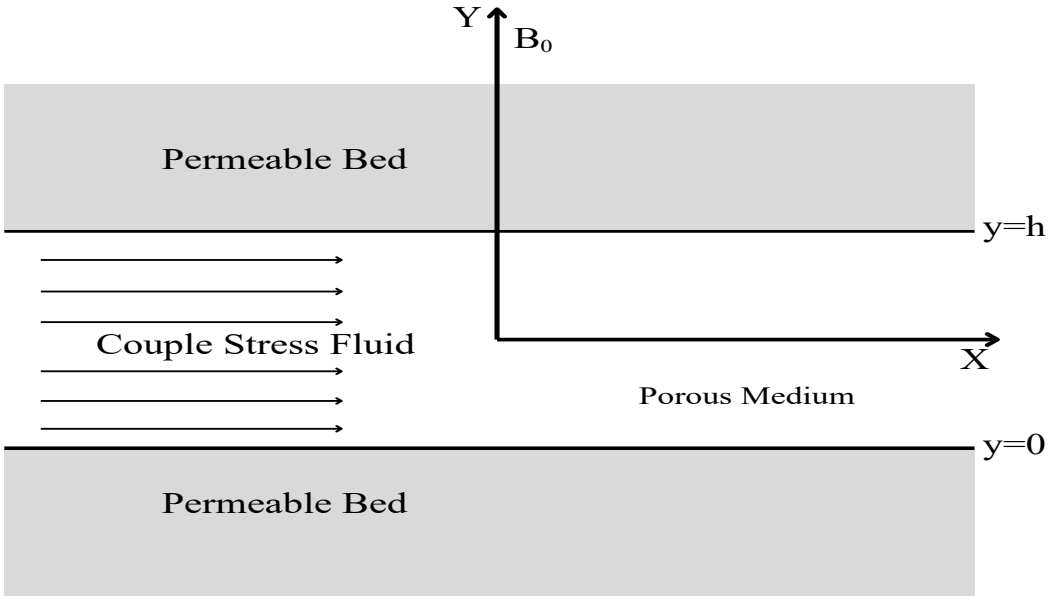

Figure 1: Flow Diagram

of strength B_0. The pressure gradient is given by

$$\frac{\partial p}{\partial x} = \left(\frac{\partial p}{\partial x}\right)_s + \left(\frac{\partial p}{\partial x}\right)_o e^{i\omega t}, \tag{2.1}$$

where $\left(\frac{\partial p}{\partial x}\right)_s$ and $\left(\frac{\partial p}{\partial x}\right)_o$ are amplitudes of steady and oscillatory pulsations, respectively, and ω is the frequency.

Let V be the velocity of constant injection from the upper permeable bed and suction from the lower permeable bed. The flow in the porous medium is modelled using Darcy-Brinkman equation, while Darcy's law is used to model the flow within the permeable beds. Since the porous medium is of high permeability, the Beaver-Joseph boundary condition is applied at the permeable beds.

The governing equations of flow [16] along with boundary conditions are

$$\frac{\partial u}{\partial x} + \frac{\partial u}{\partial y} = 0 \tag{2.2}$$

$$\frac{\partial u}{\partial t} + V\frac{\partial u}{\partial y} = -\frac{1}{\rho}\frac{\partial u}{\partial x} + \frac{\mu}{\rho}\frac{\partial^2 u}{\partial y^2} - \frac{\eta}{\rho}\frac{\partial^4 u}{\partial y^4} - \frac{\sigma B_0^2 u}{\rho} - \frac{\mu u}{\rho K} \tag{2.3}$$

$$\frac{\partial u}{\partial y} = \frac{\alpha}{\sqrt{K_1}}(u - Q_1) \;\; at \;\; y = 0 \tag{2.4}$$

$$\frac{\partial u}{\partial y} = \frac{-\alpha}{\sqrt{K_2}}(u - Q_2) \;\; at \;\; y = h \tag{2.5}$$

$$\frac{\partial^2 u}{\partial y^2} = 0 \;\; at \;\; y = 0 \tag{2.6}$$

$$\frac{\partial^2 u}{\partial y^2} = 0 \;\; at \;\; y = h, \tag{2.7}$$

where α is Beaver-Joseph constant depends on the structure of the porous medium, and $Q_1 = \frac{-K_1}{\mu}\frac{\partial p}{\partial x}$, and $Q_2 = \frac{-K_2}{\mu}\frac{\partial p}{\partial x}$ are Darcy's velocity in the lower permeable bed and upper permeable bed, respectively.

3 Non-dimensionalization of flow quantities

We introduce following non-dimensional quantities to make the governing equations and the boundary conditions dimensionless

$$x^* = \frac{x}{h}, y^* = \frac{y}{h}, u^* = \frac{u}{V}, t^* = \frac{V}{h}, p^* = \frac{p}{\rho V^2}, M = B_o h\sqrt{\frac{\sigma}{\mu_1}}$$

After dropping the asterisks, we get the governing equations of flow and boundary conditions as

$$\frac{\partial u}{\partial t} + \frac{\partial u}{\partial y} = -\frac{\partial p}{\partial x} + \frac{1}{R_e}\frac{\partial^2 u}{\partial y^2} - \frac{1}{SR_e}\frac{\partial^4 u}{\partial y^4} - \frac{M^2}{R_e}\mu - \frac{\epsilon^2}{R_e}u \tag{3.1}$$

$$\frac{\partial u}{\partial y} = \epsilon_1\alpha(u + \frac{R_e}{\epsilon_1^2}\frac{\partial p}{\partial x}) \;\; at \;\; y = 0 \tag{3.2}$$

$$\frac{\partial u}{\partial y} = -\epsilon_2\alpha(u + \frac{R_e}{\epsilon_2^2}\frac{\partial p}{\partial x}) \;\; at \;\; y = 1 \tag{3.3}$$

$$\frac{\partial^2 u}{\partial y^2} = 0 \;\; at \;\; y = 0 \tag{3.4}$$

$$\frac{\partial^2 u}{\partial y^2} = 0 \;\; at \;\; y = 1, \tag{3.5}$$

where M=$B_0 h\sqrt{\frac{\sigma}{\mu}}$, S=$\frac{\mu h^2}{\eta}$, R_e=$\frac{\rho V h}{\mu}$ and ϵ=$\frac{h}{\sqrt{K}}$ denote the Hartmann number, couple-stress parameter, the Reynolds number, and porosity parameter, respectively. ϵ_1=$\frac{h}{\sqrt{K_1}}$ and ϵ_2=$\frac{h}{\sqrt{K_2}}$ are also porosity parameters.

In view of the pulsating pressure gradient, the fluid velocity can be assumed of the form $u(y) = u_s(y) + u_o(y)e^{i\omega t}$. Substituting the value of $u(y)$ in equations 3.1 to 3.5 and separating steady and unsteady parts, the governing flow equations along with boundary conditions become

3.1 Steady Part

The governing flow equation along with boundary conditions for the steady flow is

$$\frac{1}{SR_e}\frac{d^4 u_s}{dy^4} - \frac{1}{R_e}\frac{d^2 u_s}{dy^2} + \frac{du_s}{dy} + P_s + u_s(\frac{M}{R_e} + \frac{\epsilon}{R_e}) = 0 \tag{3.6}$$

$$\frac{du_s}{dy} - \epsilon_1\alpha u_s - \frac{\alpha R_e}{\epsilon_1}(\frac{\partial p}{\partial x})_s = 0 \;\; at \;\; y = 0 \tag{3.7}$$

$$\frac{du_s}{dy} + \epsilon_2\alpha u_s - \frac{\alpha R_e}{\epsilon_2}(\frac{\partial p}{\partial x})_s = 0 \;\; at \;\; y = 1 \tag{3.8}$$

$$\frac{d^2 u_s}{dy^2} = 0 \;\; at \;\; y = 0 \tag{3.9}$$

$$\frac{d^2 u_s}{dy^2} = 0 \;\; at \;\; y = 1 \tag{3.10}$$

3.2 Oscillatory Part

The governing flow equation along with boundary conditions for the oscillatory flow is

$$\frac{1}{SR_e}\frac{d^4u_o}{dy^4} - \frac{1}{R_e}\frac{d^2u_o}{dy^2} + \frac{du_s}{dy} + P_0 + u_o(\frac{M}{R_e} + \frac{\epsilon}{R_e} + iw) = 0 \tag{3.11}$$

$$\frac{du_o}{dy} - \epsilon_1\alpha u_o - \frac{\alpha R_e}{\epsilon_1}(\frac{\partial p}{\partial x})_0 = 0 \;\; at \;\; y = 0 \tag{3.12}$$

$$\frac{du_o}{dy} + \epsilon_2\alpha u_o + \frac{\alpha R_e}{\epsilon_2}(\frac{\partial p}{\partial x})_0 = 0 \;\; at \;\; y = 1 \tag{3.13}$$

$$\frac{d^2u_o}{dy^2} = 0 \;\; at \;\; y = 0 \tag{3.14}$$

$$\frac{d^2u_o}{dy^2} = 0 \;\; at \;\; y = 1 \tag{3.15}$$

4 Solution

4.1 Steady flow solution

The solution of steady flow described in section 3.1 is given by

$$u_s(y) = C_1e^{l_1y} + C_2e^{l_2y} + C_3e^{l_3y} + C_4e^{l_4y} - \frac{A_1}{A_2}P_s, \tag{4.1}$$

where constants C_1, C_2, C_3, C_4, A_1, A_2, l_1, l_2, l_3 and l_4 are given in the Appendix.

4.2 Oscillatory flow solution

The solution of steady flow described in section 3.2 is given by

$$u_o(y) = C_5e^{l_5y} + C_6e^{l_6y} + C_7e^{l_7y} + C_8e^{l_8y} - \frac{A_1}{A_3}P_0, \tag{4.2}$$

where constants C_5, C_6, C_7, C_8, A_1, A_3, l_5, l_6, l_7 and l_8 are given in the Appendix.

4.3 Pulsatile flow solution

The solution of pulsatile flow is given by

$$u(y) = u_s(y) + u_o(y)e^{i\omega t}, \tag{4.3}$$

where $u_s(y)$ and $u_o(y)$ are given in subsections 4.1 and 4.2.

4.4 Shear stress

The shear stresses at lower and upper permeable beds in non-dimensional form, respectively, are given as

$$\tau_1 = \frac{1}{R_e}\frac{\partial u(y)}{\partial y} \quad \text{at } y = 0 \tag{4.4}$$

$$\tau_2 = \frac{1}{R_e}\frac{\partial u(y)}{\partial y} \quad \text{at } y = 1. \tag{4.5}$$

4.5 Mass flux

The instantaneous mass flux in the porous region is given by

$$Q = \int_0^1 u_s dy + \left[\int_0^1 u_o dy\right] e^{iwt} \tag{4.6}$$

5 Results and Discussion

The variations in the velocity with respect to the various physical parameters are depicted through graphs (Figures 2 – 17), for $S = 1, R_e = 2, P_s = -5, M = 1, \epsilon = 1.5, P_0 = -5, \omega = 3, \epsilon_1 = 3, \alpha = 1, \epsilon_2 = 3, t = 3$ except where they are variable. Variations in velocity for y and t simultaneously are plotted in contour plots(Figures 2 – 8). It is observed that the velocity decreases for an increase in parameters $\alpha, \epsilon, \epsilon_1, \epsilon_2, M$, while the velocity increases for an increase in the couple stress parameter S. Further, for an increase in frequency parameter ω, no change in the velocity is noticed, but the number of oscillations increases.

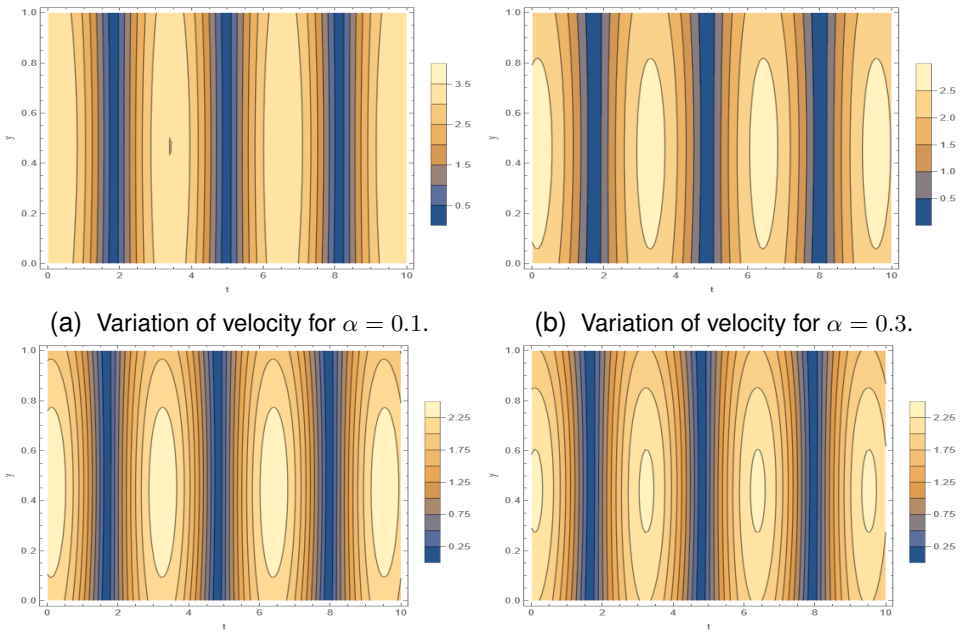

(a) Variation of velocity for $\alpha = 0.1$.

(b) Variation of velocity for $\alpha = 0.3$.

(c) Variation of velocity for $\alpha = 0.5$.

(d) Variation of velocity for $\alpha = 0.7$.

Figure 2: Variation of velocity for α

Figure 9 shows velocity variations with respect to the Beaver-Joseph constant α. The velocity decreases slowly with an increase in α, and the maximum velocity occurs at $y = 0.4$, near mid of the porous channel. Figure 10 depicts velocity variations with respect to ϵ. The velocity decreases rapidly with an increase in ϵ. The maximum velocity occurs at $y = 0.4$, near mid of the channel for $\epsilon = 1 - 3$, while for $\epsilon = 4$, we get the maximum velocity at $y = 0$. The velocity also decreases rapidly with an increase in ϵ_1 (Figure 11. The maximum velocity occurs at $y = 0$,at the lower permeable bed of the channel for $\epsilon_1 = 1 - 2$, while for $\epsilon_1 = 3 - 4$, we get the maximum velocity near mid of the

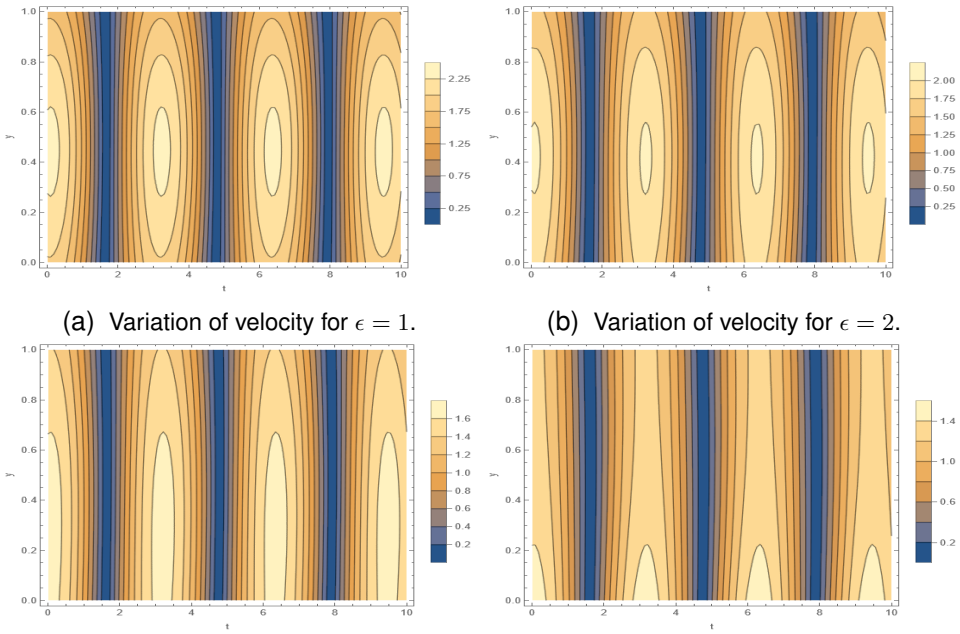

(a) Variation of velocity for $\epsilon = 1$.

(b) Variation of velocity for $\epsilon = 2$.

(c) Variation of velocity for $\epsilon = 3$.

(d) Variation of velocity for $\epsilon = 4$.

Figure 3: Variation of velocity for ϵ

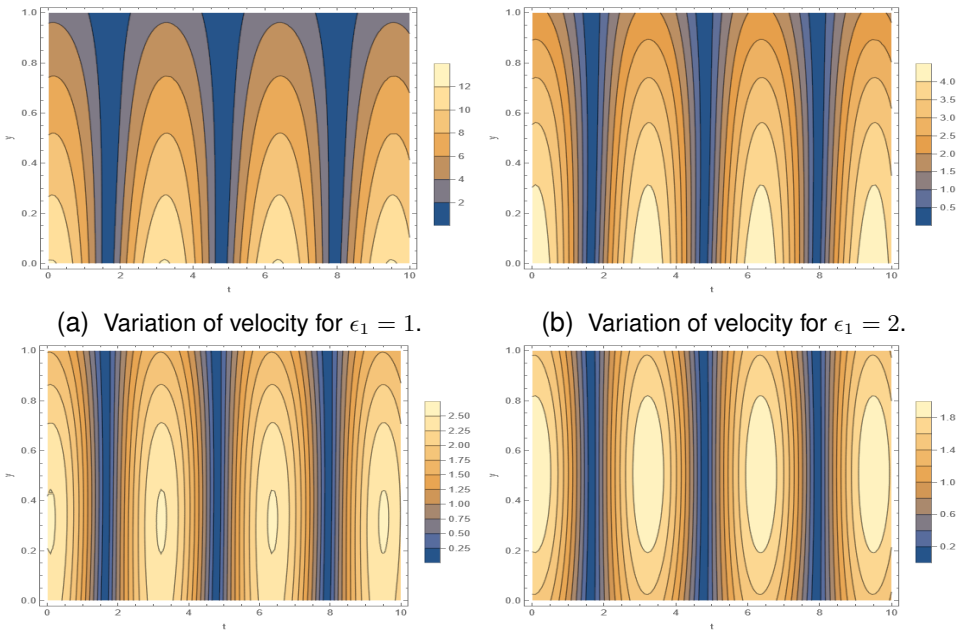

(a) Variation of velocity for $\epsilon_1 = 1$.

(b) Variation of velocity for $\epsilon_1 = 2$.

(c) Variation of velocity for $\epsilon_1 = 3$.

(d) Variation of velocity for $\epsilon_1 = 4$.

Figure 4: Variation of velocity for ϵ_1

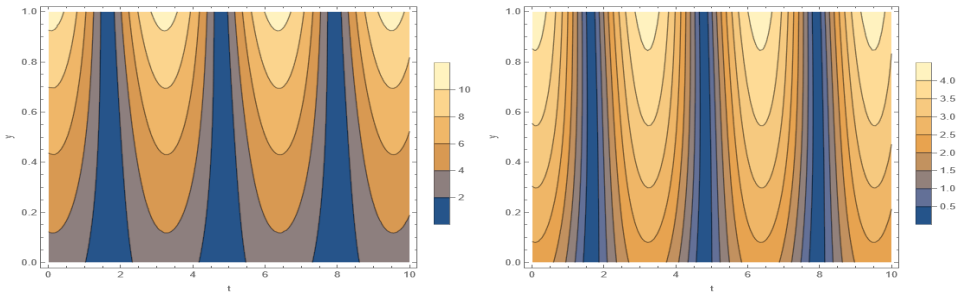

(a) Variation of velocity for $\epsilon_2 = 1$.

(b) Variation of velocity for $\epsilon_2 = 2$.

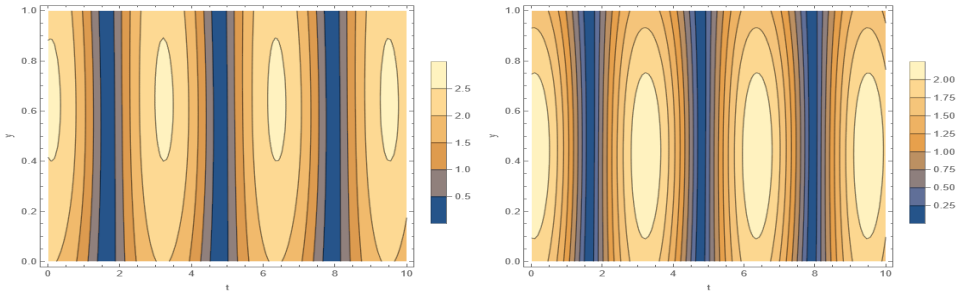

(c) Variation of velocity for $\epsilon_2 = 3$.

(d) Variation of velocity for $\epsilon_2 = 4$.

Figure 5: Variation of velocity for ϵ_2

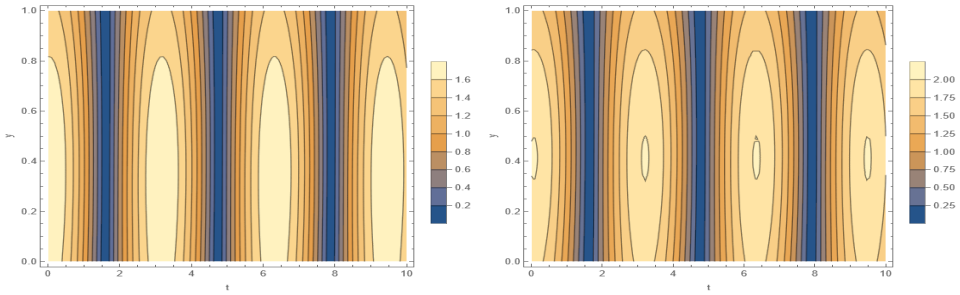

(a) Variation of velocity for $S = 1$.

(b) Variation of velocity for $S = 2$.

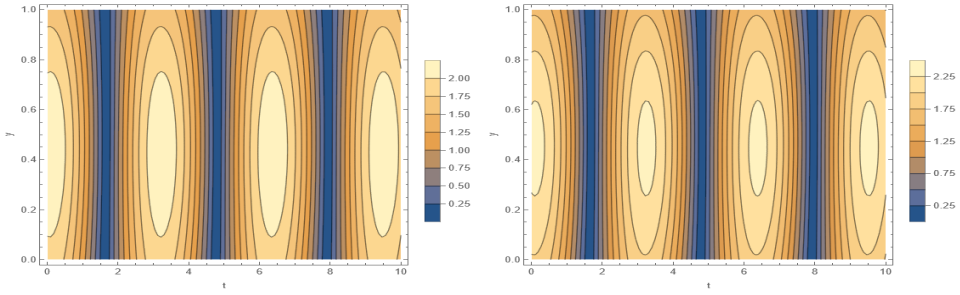

(c) Variation of velocity for $S = 3$.

(d) Variation of velocity for $S = 4$.

Figure 6: Variation of velocity for S

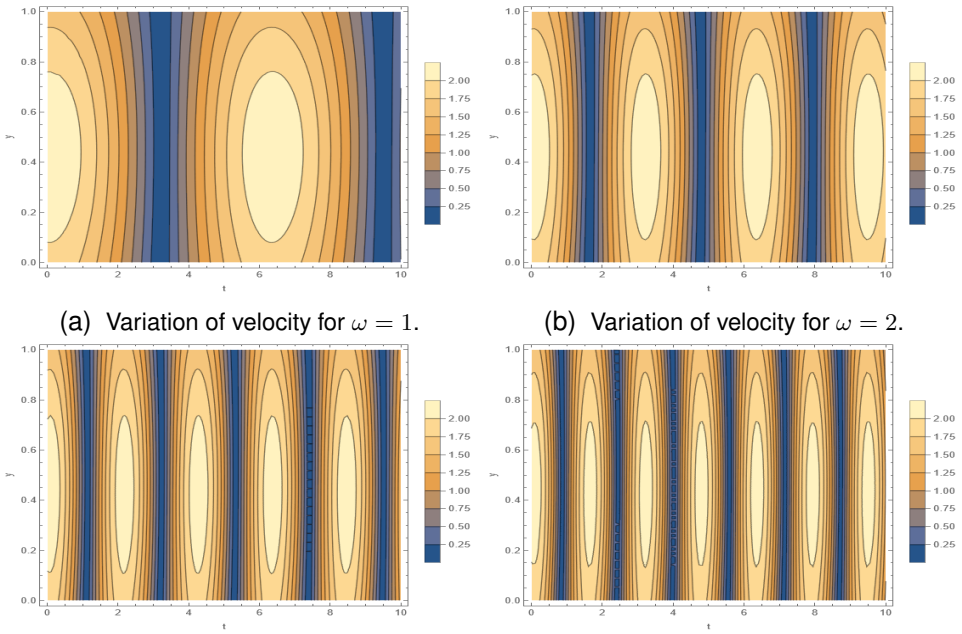

(a) Variation of velocity for $\omega = 1$.

(b) Variation of velocity for $\omega = 2$.

(c) Variation of velocity for $\omega = 3$.

(d) Variation of velocity for $\omega = 4$.

Figure 7: Variation of velocity for ω

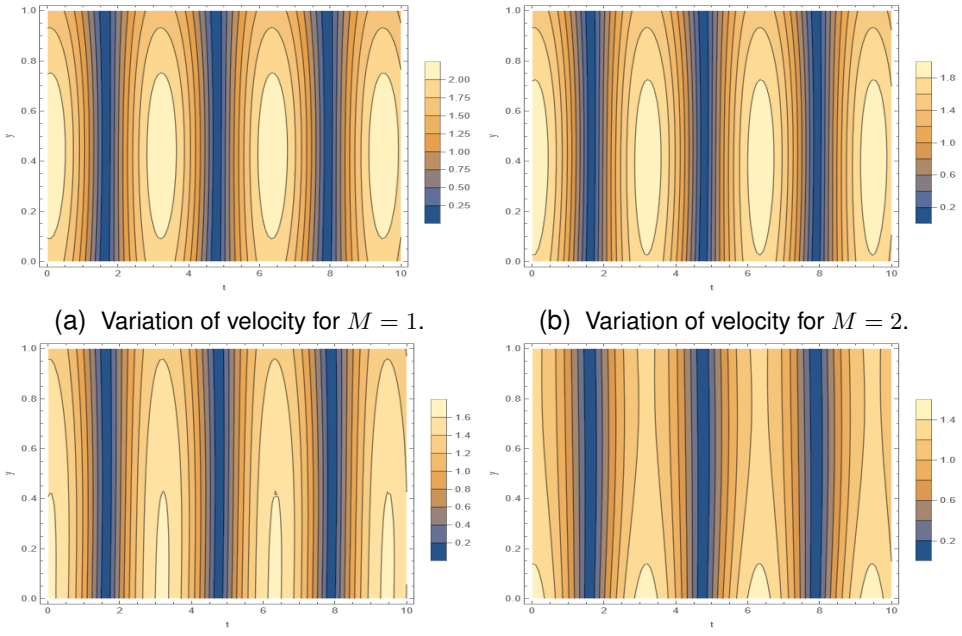

(a) Variation of velocity for $M = 1$.

(b) Variation of velocity for $M = 2$.

(c) Variation of velocity for $M = 3$.

(d) Variation of velocity for $M = 4$.

Figure 8: Variation of velocity for M

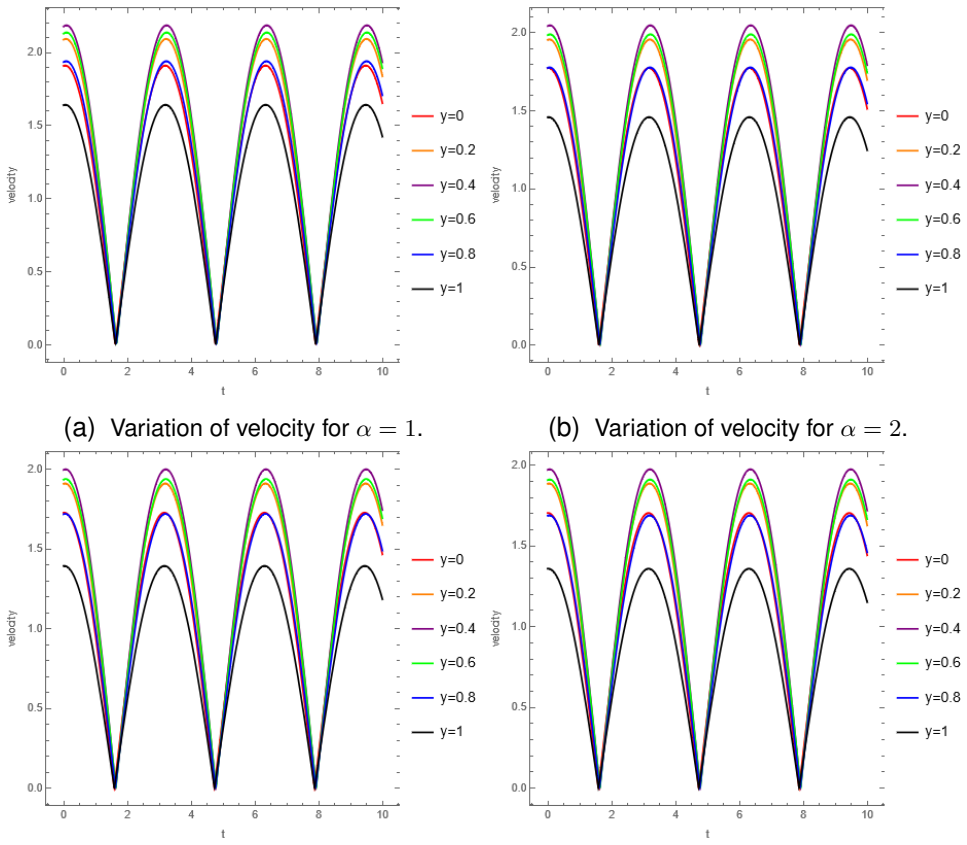

(a) Variation of velocity for $\alpha = 1$.

(b) Variation of velocity for $\alpha = 2$.

(c) Variation of velocity for $\alpha = 3$.

(d) Variation of velocity for $\alpha = 4$.

Figure 9: Variation of velocity for α

channel. Further, as ϵ_2 increases, the velocity decreases (Figure 12). The maximum velocity occurs at $y = 1$,at the upper permeable bed of the channel for $\epsilon_2 = 1 - 2$, while for $\epsilon_2 = 3 - 4$, we get the maximum velocity near mid of the channel. The velocity increases with an increase in Re and S (Figures 13, 14), and the maximum velocity occurs near mid of the channel. Figure 15 shows the variations in velocity with respect to frequency parameter ω. As ω increases, no change in velocity is noticed, but number of oscillations in the velocity profile increases. Variations in the velocity with respect to M are presented in Figure 16. An increment in M results in a decrement in the velocity. Further, we get the maximum velocity near mid of channel for $M = 1 - 2$, while for $M = 3 - 4$, the maximum velocity occurs at $y = 0$.

Figure 17 shows variations in the velocity for different values of $\epsilon, \epsilon_1, \epsilon_2, \alpha$. An increment in parameters $\epsilon, \epsilon_1, \epsilon_2, \alpha$ result in a decrement in the velocity. For $\epsilon = 1$, the velocity profile is parabolic, while for $\epsilon = 5$, the minimum velocity occurs in the mid of the channel. For $\epsilon_1 = 1$, the velocity decrement is almost linear, while for $\epsilon_2 = 1$, the velocity increment is almost linear. For all values of α, the velocity profile is parabolic.

Variations in the shear stress for $\omega t = 0, \frac{\pi}{4}, \frac{\pi}{2}$ at the permeable beds with respect to various flow parameters are presented through tables (Table: 1–6). Table 1 shows that shear stress at the lower permeable bed decreases with increase in the Reynold's number Re, while shear stress at the upper

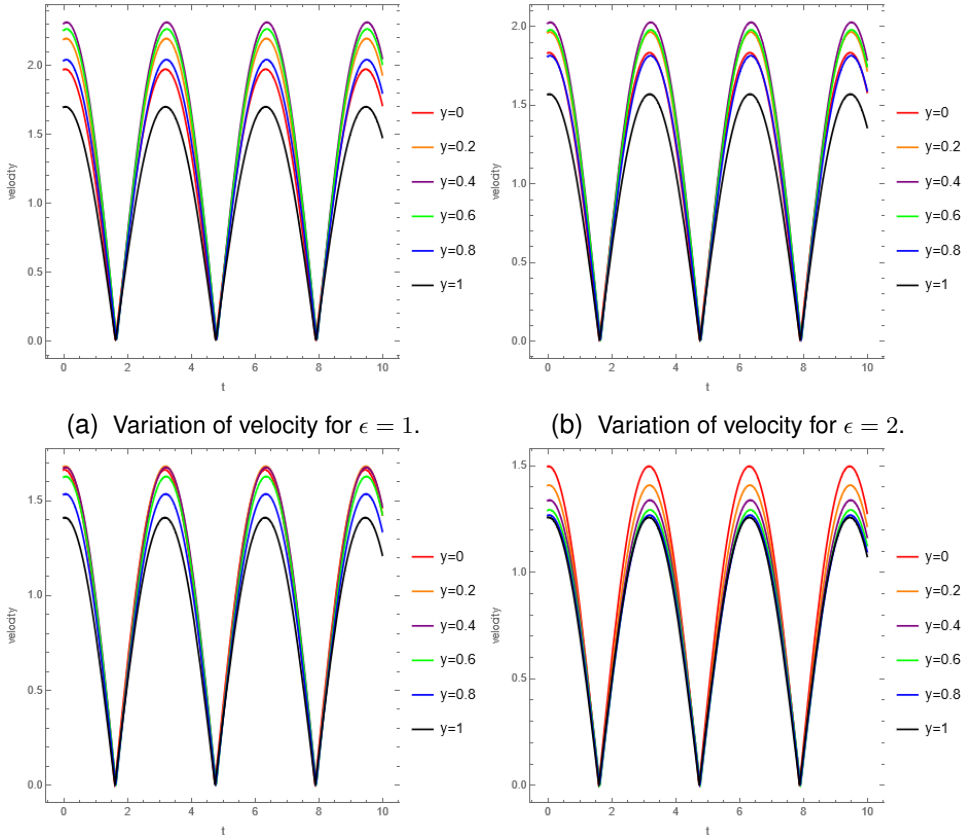

(a) Variation of velocity for $\epsilon = 1$.

(b) Variation of velocity for $\epsilon = 2$.

(c) Variation of velocity for $\epsilon = 3$.

(d) Variation of velocity for $\epsilon = 4$.

Figure 10: Variation of velocity for ϵ

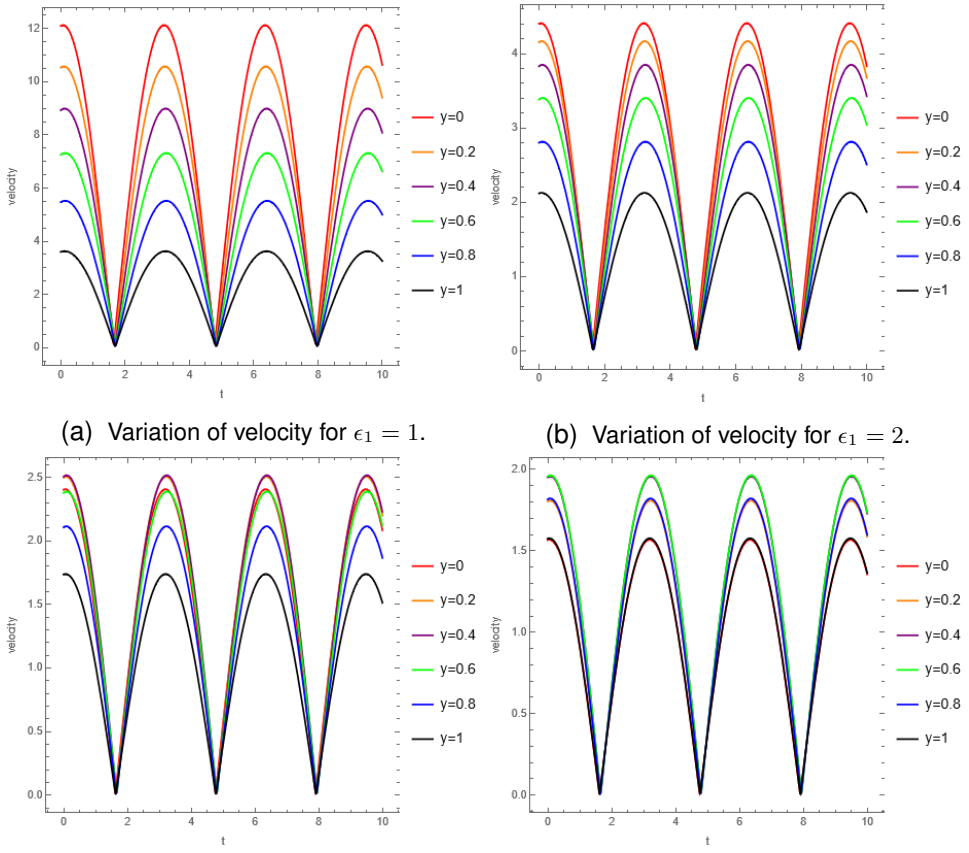

(a) Variation of velocity for $\epsilon_1 = 1$.

(b) Variation of velocity for $\epsilon_1 = 2$.

(c) Variation of velocity for $\epsilon_1 = 3$.

(d) Variation of velocity for $\epsilon_1 = 4$.

Figure 11: Variation of velocity for ϵ_1

permeable bed increases with increase in the Reynold's number Re. The shear stress at the upper permeable bed (Table:2) increases with the Hartmann number M, while at lower permeable bed, the shear stress decreases for $M = 1 - 3$, and then increases for $M = 3 - 5$. The shears stress at both the permeable beds increases with porosity parameter ϵ_1 (Table:3). For porosity parameter ϵ_2, the shear stress at lower permeable bed decreases for $\epsilon_2 = 1 - 3$, and then increases. The shear stress at the upper permeable bed decreases for $\epsilon_2 = 1 - 2$, and then increases (Table:4). Table 5 shows that shear stress at the lower permeable bed decreases with increase in the Couple Stress Parameter S, while shear stress at the upper permeable bed increases with increase in the Couple Stress Parameter S. The shear stress at both the permeable beds increases with increase in Beaver-Joseph constant (Table: 6).

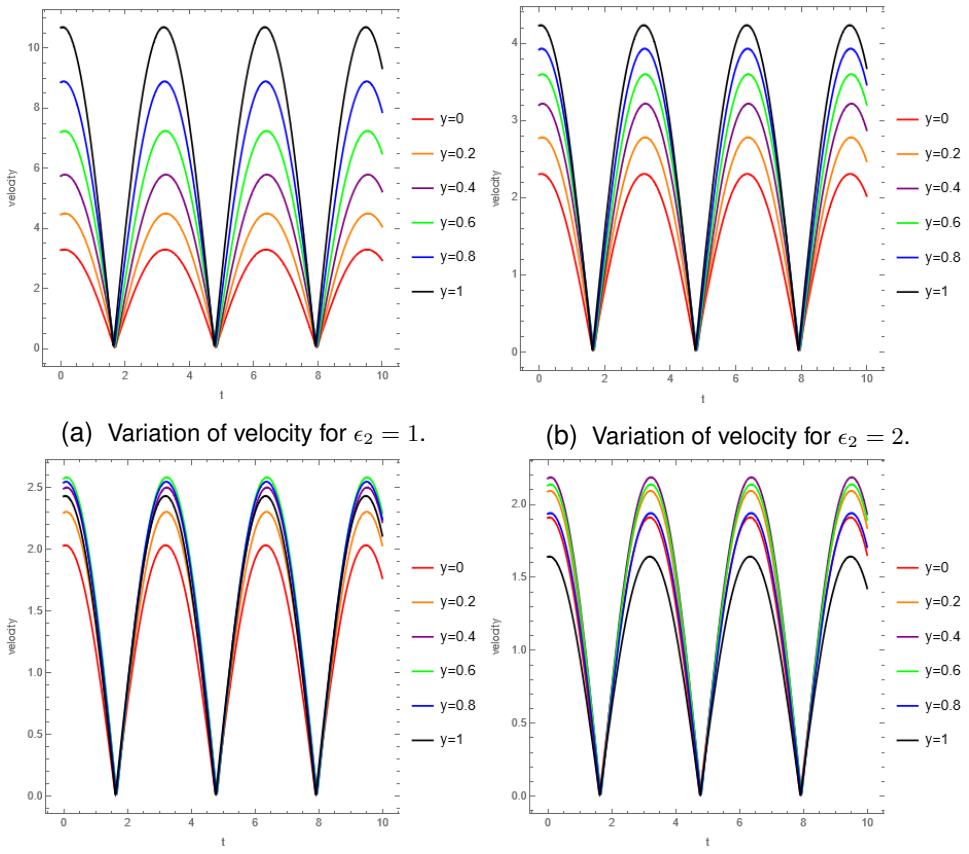

(a) Variation of velocity for $\epsilon_2 = 1$.

(b) Variation of velocity for $\epsilon_2 = 2$.

(c) Variation of velocity for $\epsilon_2 = 3$.

(d) Variation of velocity for $\epsilon_2 = 4$.

Figure 12: Variation of velocity for ϵ_2

	mod τ	$R_e = 1$	$R_e = 2$	$R_e = 3$	$R_e = 4$	$R_e = 5$
$\omega t = 0$	LPB	2.62707	2.35291	2.09098	1.84271	1.60938
	UPB	3.26771	3.46052	3.65069	3.83674	4.01746
$\omega t = \frac{\pi}{4}$	LPB	2.4641	2.24297	2.02857	1.82247	1.62612
	UPB	2.9936	3.14938	3.30572	3.46108	3.61414
$\omega t = \frac{\pi}{2}$	LPB	1.92599	1.79157	1.65734	1.52481	1.3954
	UPB	2.26374	2.35879	2.45751	2.55858	2.66076

Table 1: Variation of τ with R_e ($S = 3\ M = 1, \epsilon = 1, \epsilon_1 = 2, \epsilon_2 = 1, \alpha = 1, P_s = -5, P_O = -5$).

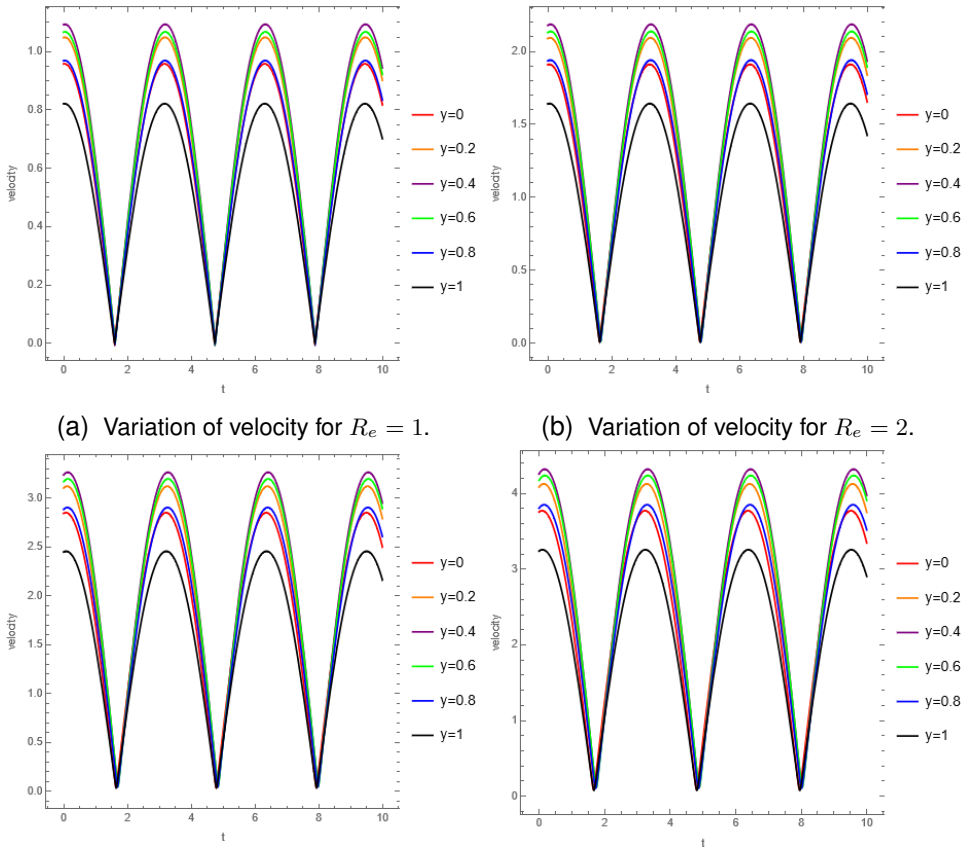

(a) Variation of velocity for $R_e = 1$.

(b) Variation of velocity for $R_e = 2$.

(c) Variation of velocity for $R_e = 3$.

(d) Variation of velocity for $R_e = 4$.

Figure 13: Variation of velocity for R_e

	mod τ	$M = 1$	$M = 2$	$M = 3$	$M = 4$	$M = 5$
$\omega t = 0$	LPB	2.35291	1.22647	0.084264	0.901437	1.59133
	UPB	3.46052	4.24105	5.06376	5.73767	6.24252
$\omega t = \frac{\pi}{4}$	LPB	2.24297	1.17924	0.0960045	0.81759	1.46149
	UPB	3.14938	3.88609	4.65922	5.28992	5.76086
$\omega t = \frac{\pi}{2}$	LPB	1.79157	0.952496	0.097595	0.609274	1.10916
	UPB	2.35879	2.93952	3.54536	4.03682	4.40216

Table 2: Variation of τ with M ($R_e = 2$ $S = 3, \epsilon = 1, \epsilon_1 = 2, \epsilon_2 = 1, \alpha = 1, P_s = -5, P_O = -5$).

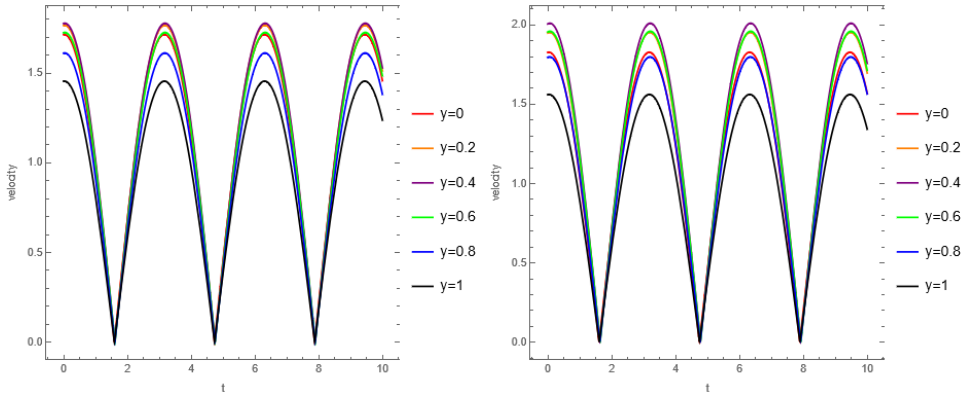

(a) Variation of velocity for $S = 1$.

(b) Variation of velocity for $S = 2$.

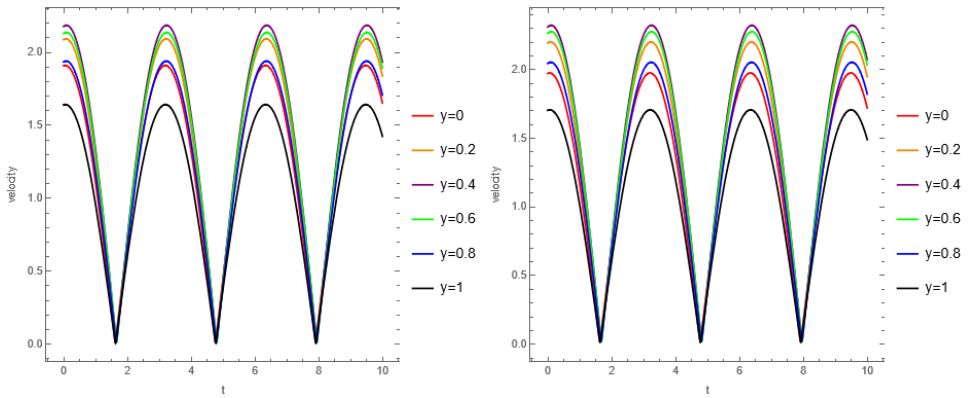

(c) Variation of velocity for $S = 3$.

(d) Variation of velocity for $S = 4$.

Figure 14: Variation of velocity for S

	mod τ	$\epsilon_1 = 1$	$\epsilon_1 = 2$	$\epsilon_1 = 3$	$\epsilon_1 = 4$	$\epsilon_1 = 5$
$\omega t = 0$	LPB	0.835348	2.35291	3.19696	3.56887	3.77341
	UPB	0.84639	3.46052	4.17818	4.4943	4.66815
$\omega t = \frac{\pi}{4}$	LPB	0.677273	2.24297	3.01134	3.34957	3.53549
	UPB	0.686235	3.14938	3.82621	4.12407	4.28781
$\omega t = \frac{\pi}{2}$	LPB	0.42072	1.79157	2.36727	2.62032	2.75933
	UPB	0.426296	2.35879	2.891474	3.12599	3.25469

Table 3: Variation of τ with ϵ_1 ($R_e = 2\ M = 1, \epsilon = 1, S = 3, \epsilon_2 = 1, \alpha = 1, P_s = -5, P_O = -5$).

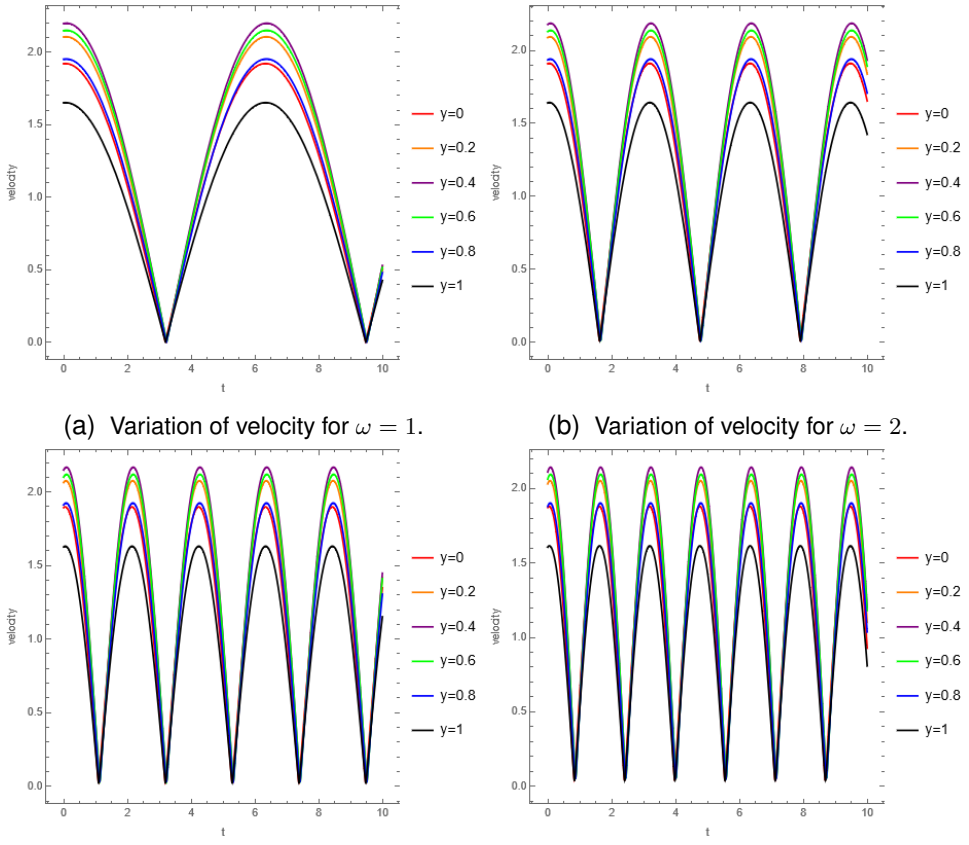

(a) Variation of velocity for $\omega = 1$.

(b) Variation of velocity for $\omega = 2$.

(c) Variation of velocity for $\omega = 3$.

(d) Variation of velocity for $\omega = 4$.

Figure 15: Variation of velocity for ω

	mod τ	$\epsilon_2 = 1$	$\epsilon_2 = 2$	$\epsilon_2 = 3$	$\epsilon_2 = 4$	$\epsilon_2 = 5$
$\omega t = 0$	LPB	2.35291	0.421484	0.154963	0.390677	0.525869
	UPB	3.46052	0.429872	1.52558	2.01987	2.29385
$\omega t = \frac{\pi}{4}$	LPB	2.24297	0.424027	0.120994	0.339434	0.466317
	UPB	3.14938	0.432471	1.44071	1.89515	2.14699
$\omega t = \frac{\pi}{2}$	LPB	1.79157	0.362106	0.0711892	0.23659	0.335795
	UPB	2.35879	0.369322	1.1365	1.4819	1.67327

Table 4: Variation of τ with ϵ_2 ($R_e = 2\ M = 1, \epsilon = 1, \epsilon_1 = 2, S = 3, \alpha = 1, P_s = -5, P_O = -5$).

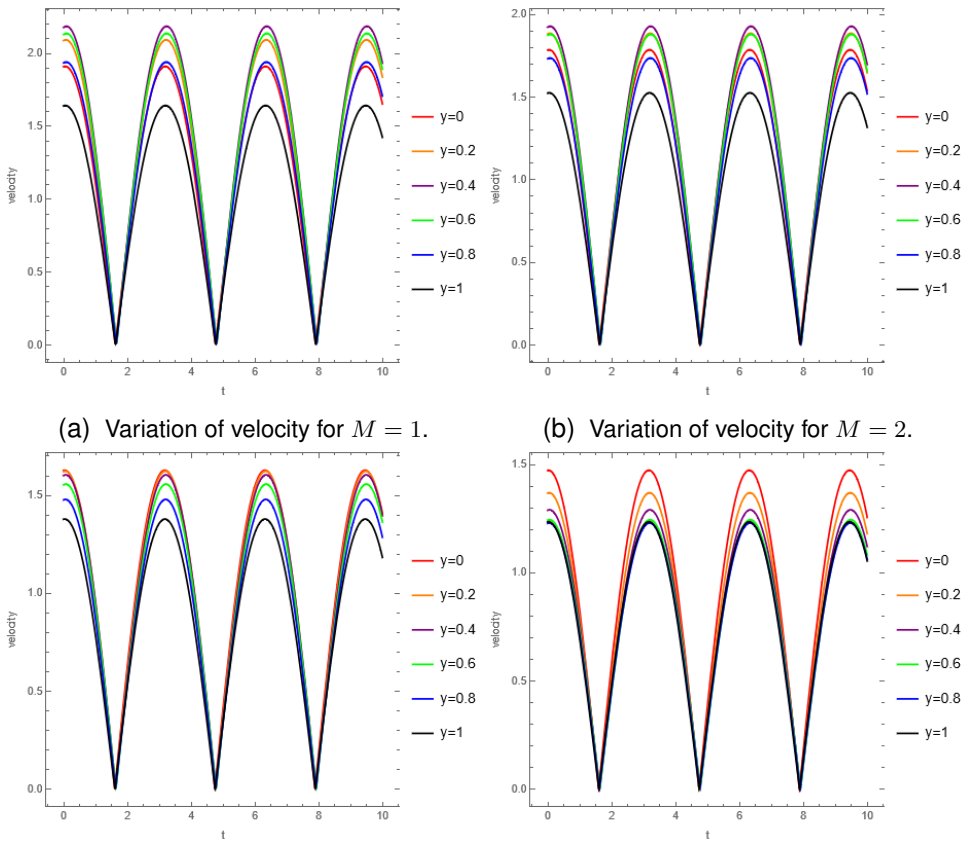

(a) Variation of velocity for $M = 1$. (b) Variation of velocity for $M = 2$.

(c) Variation of velocity for $M = 3$. (d) Variation of velocity for $M = 4$.

Figure 16: Variation of velocity for M

	mod τ	$S = 1$	$S = 2$	$S = 3$	$S = 4$	$S = 5$
$\omega t = 0$	LPB	2.71092	2.50538	2.23607	2.23607	2.14423
	UPB	3.20062	3.34792	3.46052	3.54936	3.62127
$\omega t = \frac{\pi}{4}$	LPB	2.53732	2.36889	2.24297	2.14593	2.0693
	UPB	2.93466	3.05589	3.14938	3.22365	3.28405
$\omega t = \frac{\pi}{2}$	LPB	1.97742	1.87175	1.79157	1.72909	1.67935
	UPB	2.22192	2.29862	2.35879	2.40717	2.44689

Table 5: Variation of τ with S ($R_e = 2\ M = 1, \epsilon = 1, \epsilon_1 = 2, \epsilon_2 = 1, \alpha = 1, P_s = -5, P_O = -5$).

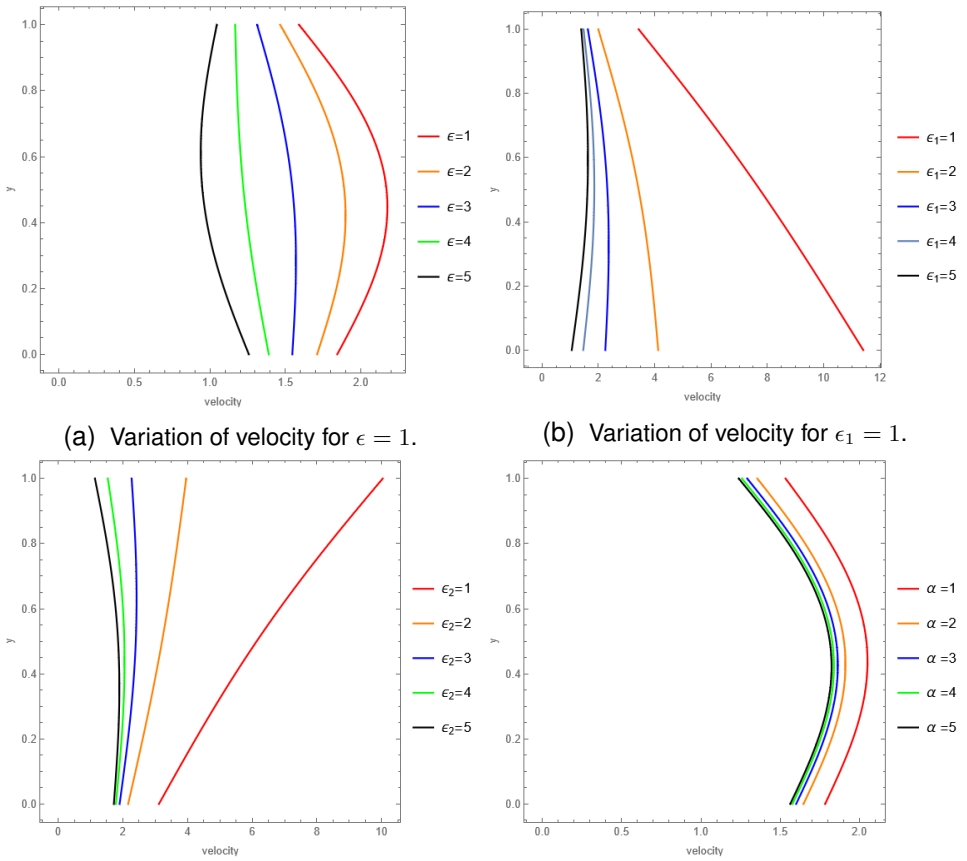

(a) Variation of velocity for $\epsilon = 1$.

(b) Variation of velocity for $\epsilon_1 = 1$.

(c) Variation of velocity for $\epsilon_2 = 1$.

(d) Variation of velocity for $\alpha = 1$.

Figure 17: Variation of velocity from different parameters

	mod τ	$\alpha = 1$	$\alpha = 2$	$\alpha = 3$	$\alpha = 4$	$\alpha = 5$
$\omega t = 0$	LPB	2.35291	3.35604	3.92435	4.29049	4.5461
	UPB	3.46052	5.03819	5.93598	6.5153	6.92005
$\omega t = \frac{\pi}{4}$	LPB	0.424027	0.440917	0.446651	0.449515	0.451228
	UPB	0.432471	0.452679	0.460086	0.463957	0.466343
$\omega t = \frac{\pi}{2}$	LPB	1.79157	2.50743	2.91134	3.17113	3.35233
	UPB	2.35879	3.45536	4.07934	4.48185	4.76301

Table 6: Variation of τ with α ($R_e = 2\ M = 1, \epsilon = 1, \epsilon_1 = 2, \epsilon_2 = 1, \S = 3, P_s = -5, P_O = -5$).

6 Conclusion

In this study, the flow of a couple-stress fluid between two permeable beds has been analysed. The exact solutions were obtained, and the results were interpreted using graphs and tables. The major conclusions drawn from the present analysis are as follows:

- The velocity decreases with increasing values of the Beaver-Joseph constant α, porosity parameters ϵ, ϵ_1, ϵ_2, and the Hartmann number M, whereas it increases with the couple stress parameter S and the Reynolds number Re.
- An increase in the frequency parameter ω does not affect the magnitude of velocity. It increases the number of oscillations in the velocity profile.
- The maximum velocity generally occurs near the mid-line of the channel. Shifts toward the permeable beds are observed for higher values of the porosity parameter and the Hartmann number.
- The velocity profile remains parabolic for lower values of porosity and permeability parameters, while significant distortion is observed at higher values.
- Shear stress at the lower permeable bed decreases with increasing Reynolds number and couple stress parameter, whereas it increases at the upper permeable bed.
- The Hartmann number increases shear stress at the upper permeable bed, while showing mixed behaviour at the lower permeable bed.
- Shear stress at both permeable beds increases with an increase in the Beavers–Joseph constant, indicating enhanced slip effects at the porous interface.

Appendix

$A_1 = SR_e$, $A_2 = (M+\epsilon)S$, $A_3 = (M+\epsilon+i\omega R_e)S$, $A_4 = B_7^2$, $A_5 = B_8^2$, $A_6 = B_7^2 e^{B_7}$, $A_7 = B_7^2 e^{-B_7}$, $A_8 = B_8^2 e^{B_8}$, $A_9 = B_8^2 e^{-B_8}$, $A_{10} = \epsilon_1\alpha - B_7$, $A_{11} = \epsilon_1\alpha + B_7$, $A_{12} = \epsilon_1\alpha - B_8$, $A_{13} = \epsilon_1\alpha + B_8$, $A_{14} = \frac{\alpha R_e}{\epsilon_1}$, $A_{15} = (\alpha\epsilon_2 + B_7)e^{B_7}$, $A_{16} = (\alpha\epsilon_2 - B_7)e^{-B_7}$, $A_{17} = (\alpha\epsilon_2 + B_8)e^{B_8}$, $A_{18} = (\alpha\epsilon_2 - B_8)e^{-B_8}$, $A_{19} = \frac{\alpha R_e}{\epsilon_2}P_s$, $A_{20} = E_7^2$, $A_{21} = E_8^2$, $A_{22} = E_7^2 e^{E_7}$, $A_{23} = E_7^2 e^{-E_7}$, $A_{24} = E_8^2 e^{E_8}$, $A_{25} = E_8^2 e^{-E_8}$, $A_{26} = \epsilon_1\alpha - E_7$, $A_{27} = \epsilon_1\alpha + E_7$, $A_{28} = \epsilon_1\alpha - E_8$, $A_{29} = \epsilon_1\alpha + E_8$, $A_{30} = \frac{\alpha R_e}{\epsilon_1}P_0$, $A_{31} = (\alpha\epsilon_2 + E_7)e^{E_7}$, $A_{32} = (\alpha\epsilon_2 - E_7)e^{-E_7}$, $A_{33} = (\alpha\epsilon_2 + E_8)e^{E_8}$, $A_{34} = (\alpha\epsilon_2 - E_8)e^{-E_8}$, $A_{35} = \frac{\alpha R_e}{\epsilon_2}$, $B_1 = S^2 + 12A_2$, $B_2 = -2S^3 + 27A_1 + 72SA_2$, $B_3 = (B_2 + \sqrt{-4(B_1)^3 + (B_2)^2})^{\frac{1}{3}}$, $B_4 = \sqrt{\frac{2S}{3} + \frac{2^{\frac{1}{3}}B_1}{B_3} + \frac{B_3}{(3)2^{\frac{1}{3}}}}$, $B_5 = \sqrt{\frac{4S}{3} - \frac{2^{\frac{1}{3}}B_1}{3B_3} - \frac{B_3}{(3)2^{\frac{1}{3}}} - \frac{2A_1}{B_4}}$, $B_6 = \sqrt{\frac{4S}{3} - \frac{2^{\frac{1}{3}}B_1}{3B_3} - \frac{B_3}{(3)2^{\frac{1}{3}}} + \frac{2A_1}{B_4}}$, $B_7 = S^2 + 12A_3$, $B_8 = -2S^3 + 27A_1^2 + 72SA_3$, $B_9 = (B_8 + \sqrt{-4B_7^3 + B_8^2})^{\frac{1}{3}}$, $B_{10} = \sqrt{\frac{4S}{3} + \frac{2^{\frac{1}{3}}B_7}{B_9} + \frac{B_9}{(3)2^{\frac{1}{3}}}}$, $B_{11} = \sqrt{\frac{4S}{3} - \frac{2^{\frac{1}{3}}B_7}{3B_9} - \frac{B_9}{(3)2^{\frac{1}{3}}} - \frac{2A_1}{B_{10}}}$, $B_{12} = \sqrt{\frac{4S}{3} - \frac{2^{\frac{1}{3}}B_7}{3B_9} - \frac{B_9}{(3)2^{\frac{1}{3}}} + \frac{2A_1}{B_{10}}}$, $l_1 = \frac{1}{2}(B_4 - B_5)$, $l_2 = \frac{1}{2}(B_4 + B_5)$, $l_3 = -\frac{1}{2}(B_4 + B_6)$, $l_4 = \frac{1}{2}(B_6 - B_4)$, $l_5 = \frac{1}{2}(B_{10} - B_{11})$, $l_6 = \frac{1}{2}(B_{10} + B_{11})$, $l_7 = -\frac{1}{2}(B_{10} + B_{12})$, $l_8 = \frac{1}{2}(B_{12} - B_{10})$, $A_5A_8 - A_6A_9 = M_1$, $A_5A_{16} - A_4A_{18} = M_2$, $A_5A_7 - A_4A_9 = M_3$, $A_5A_{17} - A_5A_{18} = M_4$, $A_5A_{11} - A_4A_{13} = M_5$, $A_5A_{12} - A_5A_{13} = M_6$, $A_5A_{15} - A_4A_{18} = M_7$, $A_5A_6 - A_4A_9 = M_8$, $A_5A_{10} - A_4A_{13} = M_9$, $(M_1M_2 - M_3M_4) = M_{10}$, $(M_1M_5 - M_3M_6) = M_{11}$, $(M_1M_7 - M_8M_4) = M_{12}$, $(M_1M_9 - M_8M_6) = M_{13}$, $(M_{11}M_{12} - M_{13}M_{10}) = M_{14}$, $(-A_5M_1A_{14}M_{10} + A_5M_1M_{11}A_{19} = M_{15})$, $A_5A_8A_{14}A_{15} - A_5A_9A_{14}A_{15} = M_{16}$, $-A_5A_6A_{14}A_{17} + A_4A_9A_{14}A_{17} = M_{17}$, $A_5A_6A_{14}A_{18} - A_4A_8A_{14}A_{18} = M_{18}$, $-A_5A_8A_{10}A_{19} + A_5A_9A_{10}A_{19} = M_{19}$, $A_5A_6A_{12}A_{19} - A_4A_9A_{12}A_{19} = M_{20}$, $-A_5A_6A_{13}A_{19} + A_4A_8A_{13}A_{19} = M_{21}$, $A_5A_8A_{11}A_{15} - A_5A_9A_{11}A_{15} = M_{22}$,

$-A_5A_7A_{12}A_{15}+A_4A_9A_{12}A_{15}=M_{23}$, $A_5A_7A_{13}A_{15}-A_4A_8A_{13}A_{15}=M_{24}$, $-A_5A_8A_{10}A_{16}+A_5A_9A_{10}A_{16}=M_{25}$, $A_5A_6A_{12}A_{16}-A_4A_9A_{12}A_{16}=M_{26}$, $-A_5A_6A_{13}A_{16}+A_4A_8A_{13}A_{16}=M_{27}$, $A_5A_7A_{10}A_{17}-A_4A_9A_{10}A_{17}=M_{28}$, $-A_5A_6A_{11}A_{11}+A_4A_9A_{11}A_{17}=M_{29}$, $A_4A_6A_{13}A_{17}-A_4A_4A_{13}A_{17}=M_{30}$, $-A_5A_7A_{10}A_{18}+A_4A_8A_{10}A_{18}=M_{31}$, $A_5A_6A_{11}A_{18}-A_4A_8A_{11}A_{18}=M_{32}$, $-A_4A_6A_{12}A_{18}+A_4A_7A_{12}A_{18}=M_{33}$, $M_{16}M_{17}+M_{18}M_{19}+M_{20}M_{21}=M_{34}$, $M_{22}M_{23}+M_{24}M_{25}=M_{35}$, $M_{26}M_{27}+M_{28}M_{29}=M_{36}$, $M_{30}M_{31}+M_{32}M_{33}=M_{37}$, $M_{35}+M_{36}+M_{37}=M_{38}4$, $A_5A_7A_{14}A_{15}-A_4A_9A_{14}A_{15}=M_{39}$, $-A_5A_6A_{14}A_{16}+A_4A_9A_{14}A_{16}=M_{40}$, $A_4A_6A_{14}A_{18}-A_4A_7A_{14}A_{18}=M_{41}$, $-A_5A_7A_{10}A_{19}+A_4A_9A_{10}A_{19}=M_{42}$, $A_5A_6A_{11}A_{19}-A_4A_9A_{11}A_{19}=M_{43}$, $-A_4A_6A_{13}A_{19}+A_4A_7A_{13}A_{19}=M_{44}$, $-A_5A_8A_{11}A_{15}+A_5A_9A_{11}A_{15}=M_{45}$, $A_5A_7A_{12}A_{15}-A_4A_9A_{12}A_{15}=M_{46}$, $-A_5A_7A_{13}A_{15}+A_4A_8A_{12}A_{15}=M_{47}$, $A_5A_8A_{10}A_{16}-A_5A_9A_{10}A_{16}=M_{48}$, $-A_5A_6A_{12}A_{16}+A_4A_9A_{12}A_{16}=M_{49}$, $A_5A_6A_{13}A_{16}-A_4A_8A_{13}A_{16}=M_{50}$, $-A_5A_7A_{10}A_{17}+A_4A_9A_{10}A_{17}=M_{51}$, $A_5A_6A_{11}A_{17}-A_4A_9A_{11}A_{17}=M_{52}$, $-A_4A_6A_{13}A_{17}+A_4A_7A_{13}A_{17}=M_{53}$, $A_5A_7A_{10}A_{18}-A_4A_8A_{10}A_{18}=M_{54}$, $-A_5A_6A_{11}A_{18}+A_4A_8A_{11}A_{18}=M_{55}$, $A_4A_6A_{12}A_{18}-A_4A_7A_{12}A_{18}=M_{56}$, $M_{39}M_{40}+M_{41}M_{42}+M_{43}M_{44}=M_{57}$, $M_{45}+M_{46}M_{47}+M_{48}M_{49}+M_{50}M_{51}+M_{52}M_{53}+M_{54}M_{55}+M_{56}=M_{58}$, $-A_5A_7A_{14}A_{15}+A_4A_8A_{14}A_{15}=M_{59}$, $A_5A_6A_{14}A_{16}-A_4A_8A_{14}A_{16}=M_{60}$, $-A_4A_6A_{14}A_{17}+A_4A_7A_{14}A_{17}=M_{61}$, $A_5A_7A_{10}A_{19}-A_4A_8A_{10}A_{19}=M_{62}$, $-A_5A_6A_{11}A_{19}+A_4A_8A_{11}A_{19}=M_{63}$, $A_4A_6A_{12}A_{19}-A_4A_7A_{12}A_{19}=M_{64}$, $M_{59}+M_{60}M_{61}+M_{62}M_{63}+M_{64}=M_{65}$, $A_{21}A_{24}-A_{21}A_{25}=N_1$, $A_{21}A_{32}-A_{20}A_{34}=N_2$, $A_{21}A_{23}-A_{20}A_{25}=N_3$, $A_{21}A_{33}-A_{21}A_{34}=N_4$, $A_{21}A_{27}-A_{20}A_{29}=N_5$, $A_{21}A_{28}-A_{21}A_{29}=N_6$, $A_{21}A_{31}-A_{20}A_{34}=N_7$, $A_{21}A_{22}-A_{20}A_{25}=N_8$, $A_{21}A_{26}-A_{20}A_{29}=N_9$, $(N_1N_2-N_3N_4)=N_{10}$, $(N_1N_5-N_3N_6)=N_{11}$, $(N_1N_7-N_8N_4)=N_{12}$, $(N_1N_9-N_8N_6)=N_{13}$, $(-A_{21}N_1A_{30}N_{10}+A_{21}N_1N_{11}A_{35})=N_{14}$, $(N_{11}N_{12}-N_{13}N_{10})=N_{14}$, $A_{21}A_{24}A_{30}A_{31}-A_{21}A_{25}A_{30}A_{31}=N_{16}$, $-A_{21}A_{22}A_{30}A_{33}+A_{20}A_{25}A_{30}A_{33}=N_{17}$, $A_{21}A_{22}A_{30}A_{34}-A_{20}A_{24}A_{30}A_{34}=N_{18}$, $-A_{21}A_{24}A_{26}A_{35}+A_{21}A_{25}A_{26}A_{35}=N_{19}$, $A_{21}A_{22}A_{28}A_{35}-A_{20}A_{25}A_{28}A_{35}=N_{20}$, $-A_{21}A_{22}A_{29}A_{35}+A_{20}A_{24}A_{29}A_{35}=N_{21}$, $A_{21}A_{24}A_{27}A_{31}-A_{21}A_{25}A_{27}A_{31}=N_{22}$, $-A_{21}A_{23}A_{28}A_{31}+A_{20}A_{25}A_{28}A_{31}=N_{23}$, $A_{21}A_{23}A_{29}A_{31}-A_{20}A_{24}A_{29}A_{31}=N_{24}$, $-A_{21}A_{24}A_{26}A_{32}+A_{21}A_{25}A_{26}A_{32}=N_{25}$, $A_{21}A_{22}A_{28}A_{32}-A_{20}A_{25}A_{28}A_{32}=N_{26}$, $-A_{21}A_{22}A_{29}A_{32}+A_{20}A_{24}A_{29}A_{32}=N_{27}$, $A_{21}A_{23}A_{26}A_{33}-A_{20}A_{25}A_{26}A_{33}=N_{28}$, $-A_{21}A_{22}A_{27}A_{33}+A_{20}A_{25}A_{27}A_{33}=N_{29}$, $A_{20}A_{22}A_{29}A_{33}-A_{20}A_{23}A_{29}A_{33}=N_{30}$, $-A_{21}A_{23}A_{26}A_{34}+A_{20}A_{24}A_{26}A_{34}=N_{31}$, $A_{21}A_{22}A_{27}A_{34}-A_{20}A_{24}A_{27}A_{34}=N_{32}$, $-A_{20}A_{22}A_{28}A_{34}+A_{20}A_{23}A_{28}A_{34}=N_{33}$, $(N_{16}N_{17}+N_{18}N_{19}+N_{20}N_{21})=N_{34}$, $(N_{22}N_{23}+N_{24}N_{25}+N_{26}N_{27}+N_{28}N_{29}+N_{30}N_{31}+N_{32}N_{33})=N_{35}$, $A_{21}A_{23}A_{30}A_{31}-A_{20}A_{25}A_{30}A_{31}=N_{36}$, $-A_{21}A_{22}A_{30}A_{32}+A_{20}A_{25}A_{30}A_{32}=N_{37}$, $A_{20}A_{22}A_{30}A_{34}-A_{20}A_{23}A_{30}A_{34}=N_{38}$, $-A_{21}A_{23}A_{26}A_{35}+A_{20}A_{25}A_{26}A_{35}=N_{39}$, $A_{21}A_{22}A_{27}A_{35}-A_{20}A_{25}A_{27}A_{35}=N_{40}$, $-A_{20}A_{22}A_{29}A_{35}+A_{20}A_{23}A_{29}A_{35}=N_{41}$, $-A_{21}A_{24}A_{27}A_{31}+A_{21}A_{25}A_{27}A_{31}=N_{42}$, $A_{21}A_{23}A_{28}A_{31}-A_{20}A_{25}A_{28}A_{31}=N_{43}$, $-A_{21}A_{23}A_{29}A_{31}+A_{20}A_{24}A_{29}A_{31}=N_{44}$, $A_{21}A_{24}A_{26}A_{32}-A_{21}A_{25}A_{26}A_{32}=N_{45}$, $-A_{21}A_{22}A_{28}A_{32}+A_{20}A_{25}A_{28}A_{32}=N_{46}$, $A_{21}A_{22}A_{29}A_{32}-A_{20}A_{24}A_{29}A_{32}=N_{47}$, $-A_{21}A_{23}A_{26}A_{33}+A_{20}A_{25}A_{26}A_{33}=N_{48}$, $A_{21}A_{22}A_{27}A_{33}-A_{20}A_{25}A_{27}A_{33}=N_{49}$, $-A_{20}A_{22}A_{29}A_{33}+A_{20}A_{23}A_{29}A_{33}=N_{50}$, $A_{21}A_{23}A_{26}A_{34}-A_{20}A_{24}A_{26}A_{34}=N_{51}$, $-A_{21}A_{22}A_{27}A_{34}+A_{20}A_{24}A_{27}A_{34}=N_{52}$, $A_{20}A_{22}A_{28}A_{34}-A_{20}A_{23}A_{28}A_{34}=N_{53}$, $(N_{36}N_{37}+N_{38}N_{39}+N_{40}N_{41})=N_{54}$, $(N_{42}+N_{43}N_{44}+N_{45}N_{46}+N_{47}N_{48}+N_{49}N_{50}+N_{51}N_{52}+N_{53})=N_{55}$, $-A_{21}A_{23}A_{30}A_{31}+A_{20}A_{24}A_{30}A_{31}=N_{56}$, $A_{21}A_{22}A_{30}A_{32}-A_{20}A_{24}A_{30}A_{32}=N_{57}$, $-A_{20}A_{22}A_{30}A_{33}+A_{20}A_{23}A_{30}A_{33}=N_{58}$, $A_{21}A_{23}A_{26}A_{35}-A_{20}A_{24}A_{26}A_{35}=N_{59}$, $-A_{21}A_{22}A_{27}A_{35}+A_{20}A_{24}A_{27}A_{35}=N_{60}$, $A_{20}A_{22}A_{28}A_{35}-A_{20}A_{23}A_{28}A_{35}=N_{61}$, $(N_{56}N_{57}N_{58}+N_{59}N_{60}+N_{61})=N_{62}$, $-(\frac{M_{15}}{M_{14}})=C_1$, $-(\frac{M_{34}}{M_{38}})=C_2$, $-(\frac{M_{57}}{M_{58}})=C_3$, $-(\frac{M_{65}}{M_{58}})=C_4$, $-(\frac{N_{14}}{N_{15}})=C_5$, $-(\frac{N_{34}}{N_{35}})=C_6$, $-(\frac{N_{54}}{N_{55}})=C_7$, $-(\frac{N_{62}}{N_{55}})=C_8$,

References

[1] Beavers, G. and Joseph, D. D. (1967). Boundary conditions at naturally permeable wall, *J. Fluid Mech.*. 30(1): 197–207.

[2] Wang, Y.C. (1971). Pulsatile flow in a porous channel. *Trans ASME, J. Appl. Mech.*, 38: 553–555.

[3] Rudraiah N. et.al.(1975). Hartmann flow over a permeable bed. *Int J Eng Sci.*,13(1): 1–24.

[4] Radhakrishnamacharya, G. and M.K. Maiti (1977). Heat transfer to pulsatile flow in a porous channel. Int. *J. Heat Mass Trans.*, 20: 171–173.

[5] Chandra, P. and J.S.V.R.K. Prasad (1994). Pulsatile flow in circular tubes of varying cross-section with suction/injection. *J. Aust. Math. Soc. Ser. B*, 35: 366–381.

[6] Elsoud,et.al.(1998).Interaction of peristaltic flow with pulsatile cople-stress fluid.*J.Biomath.*,13:417–425.

[7] Vajravelu,et.al.(2003). Pulsatile flow between permeable beds. *Int. J. Non-Linear Mech.*, 38:999–1005.

[8] Afifi,N.A.S and Gad,N.S.(2003).Interaction of peristaltic Flow with pulsatile fluid through a porous medium.*App.Math.and Comp.*,142:167–176.

[9] T. Malathy, S. Srinivas (2008). Pulsatile flow of a hydromagnetic fluid between permeable beds. *Int. Comm. In Heat and Mass Transfer*,35: 681-688.

[10] Pantokratoras A, Fang T.(2010). Flow of a weakly conducting fluid in a channel filled with a porous medium. *Transp Porous Media*,83:667–676.

[11] B.G.Prasad and A.Kumar (2011). Flow of a hydromagnetic fluid through porous media between permeable beds under exponentially decaying pressure gradient.*comput.Math.Sci.Technol*,17(1–2):63–74.

[12] Avinash.K,et.al.(2011). Pulsatile flow of viscous stratified fluid of variable viscosity between permeable beds.*Jr.of Porous Media*,14(12):2011,1115–1124.

[13] Srinivasacharya D, Rao G. M (2015). MHD effect on the couple stress fluid flow through a bifurcated artery. *Procedia Eng.* 127: 877–884.

[14] Aparna P,et.al.(2020). Couple Stress Fluid flow due to slow steady oscillations of a permeable sphere.*Nonlinear Eng.*,9(1):352–360.

[15] Baranovskii ES, et.al.(2021). Exact solutions to the Navier–Stokes equations with couple stresses. *Symmetry*, 13(8):1355.

[16] Kumar, D. and Agarwal, M. (2021). MHD pulsatile flow and heat transfer of two immiscible couple stress fluids between permeable beds. *Kyungpook Mathematical Journal*, 61(2): 323–351.

[17] Abbas Z, et.al. (2022). Rheology of peristaltic flow in couple stress fluid in an inclined tube heat and mass transfer analysis.*(*Adv Mech Eng.), 14(11):168781322211399.

[18] Tarakaramu N, et.al.(2022). Three-dimensional non-Newtonian couple stress fluid flow over a permeable stretching surface with nonlinear thermal radiation and heat source effects. *Heat Transfer*, 51(6).5348–5367.

[19] Alsudais NS, et.al.(2022). Stokes flow of an incompressible couple stress fluid confined between two eccentric spheres.*Eur J Mech B/Fluids*, 91: 244–252.

[20] Bansal, S., Yadav, R. S. (2024). Effect of slip velocity on Newtonian fluid flow induced by a stretching surface within a porous medium. *Journal of Engineering and Applied Science*, 71(1), 153.

[21] Dhwal, S. R.,et.al. (2025). Numerical study of radiating Casson fluid past a permeable stretching sheet in a Darcy-Forchheimer porous medium. *Archives of Thermodynamics*, 199–208.